Numerical Heat Transfer, Part A, 46: 181–198, 2004

ISSN: 1040-7782 print/1521-0634 online
DOI: 10.1080/10407780490463845

Taylor & Francis
Taylor & Francis Group

SIMULTANEOUS HEAT AND MASS TRANSFER FROM A PERMEABLE SPHERE AT UNIFORM HEAT AND MASS FLUXES WITH MAGNETIC FIELD AND RADIATION EFFECTS

Ali J. Chamkha and Ali Al-Mudhaf
Manufacturing Engineering Department, The Public Authority for Applied Education and Training, Shuweikh, Kuwait

The problem of coupled heat and mass transfer by natural convection from a permeable sphere in the presence of an external magnetic field and thermal radiation effects is formulated. The sphere surface is maintained at a constant heat and mass fluxes and is permeable to allow for possible fluid wall suction or blowing. The resulting governing equations are nondimensionalized and transformed into a nonsimilar form and then solved numerically by an implicit, iterative, finite-difference method. Comparisons with previously published work are performed and excellent agreement is obtained. A parametric study of the physical parameters is conducted and a representative set of numerical results for the velocity, temperature, and concentration profiles as well as the local skin-friction coefficient, local wall temperature, and local wall concentration is illustrated graphically to show interesting features of the solutions.

INTRODUCTION

Coupled heat and mass transfer finds applications in a variety of engineering processes such as heat exchanger devices, petroleum reservoirs, chemical catalytic reactors and processes, nuclear waste repositories, and others. The steady laminar flow and forced-convection heat transfer on a rotating sphere with its axis of rotation parallel to the free-stream velocity has been studied by a number of previous investigators [1–4]. Siekann [1] reported on the calculation of the thermal boundary layer on a rotating sphere. Chao and Grief [2] and Lee et al. [3] considered laminar forced-convection boundary-layer flow over rotating bodies. Kumari and Nath [4] studied nonsimilar incompressible boundary-layer flow over a rotating sphere. Chen and Mucoglu [5] analyzed steady mixed-convection flow over stationary spheres with uniform wall temperatures, while Mucoglu and Chen [6] considered the same problem with uniform wall heat flux. Fendell [7] analyzed laminar natural convection about an isothermally heated sphere at small Grashof numbers. Potter and Riley [8] extended the problem of Fendell [7] to large Grashof numbers. Hieber and Gebhart

Received 7 November 2003; accepted 6 March 2004.
Address correspondence to Ali J. Chamkha, Manufacturing Engineering Department, The Public Authority for Applied Education and Training, P.O. Box 42325, Shuweikh, 70654 Kuwait. E-mail: chamkha@paaet.edu.kw

NOMENCLATURE

a	radius of the sphere	r	radial coordinate $\{= a[\sin(x/a)]\}$
B_0	magnetic induction	Sc	Schmidt number $(= \nu/D)$
c	concentration	Sh	Sherwood number $(= h_m a/D)$
c_p	specific heat at constant pressure	T	temperature
C	dimensionless concentration $[=(c - c_\infty)D(\mathrm{Gr})^{1/5}/(am_w)]$	u	velocity in the x direction
		v	velocity in the y direction
C_f	local skin-friction coefficient, Eq. (20)	v_w	suction or injection velocity
D	mass diffusivity	x	streamwise coordinate
f	dimensionless stream function $\{=\psi/[\nu\xi(\mathrm{Gr})^{1/5}]\}$	y	transverse coordinate
		β_c	coefficient of concentration expansion
f_0	transpiration or suction/injection parameter $\{= -v_w a/[\nu(\mathrm{Gr})^{1/5}]\}$	β_T	coefficient of thermal expansion
		η	pseudo-similarity variable $[=y(\mathrm{Gr})^{1/5}/a]$
g	gravitational acceleration		
Gr	Grashof number $[= g\beta_T q_w a^4/(k^2\nu)]$	θ	dimensionless temperature $[=(T - T_\infty)k(\mathrm{Gr})^{1/5}/(aq_w)]$
h	heat transfer coefficient		
h_m	mass transfer coefficient		
Ha^2	square of Hartmann number $\{= \sigma B_0^2 a^2/[\rho\nu(\mathrm{Gr})^{2/5}]\}$	ν	kinematic viscosity
		ρ	fluid density
k	fluid thermal conductivity	σ	electrical conductivity
K_1	mean absorption coefficient	σ_1	Stefan-Boltzmann constant
m_w	wall mass flux	ξ	dimensionless circumferential coordinate $(= x/a)$
N	buoyancy ratio $[= \beta_c m_w k/(\beta_T q_w D)]$		
N_R	radiation parameter $[kK_1/(4\sigma_1 T_\infty^3)]$	ψ	stream function
Nu	Nusselt number $(= ha/k)$		
Pr	Prandtl number $(= \rho\nu c_p/k)$		
q_r	radiative heat flux $[= -4\sigma_1/(3K_1)\partial(T^4)/\partial y]$	**Subscripts**	
		w	condition at the wall
q_w	wall heat flux	∞	condition at free stream

[9] analyzed the mixed-convection flow around a heated sphere at small Reynolds and Grashof numbers. Riley [10] studied the heat transfer from a sphere in free convective flow. Geoola and Cornish [11, 12] reported numerical solutions for free-convective heat transfer from a sphere. Jia and Gogos [13] considered laminar natural convection from isothermal spheres. Singh and Hasan [14] studied free convection about a sphere at small Grashof numbers. Kocabiyik [15] studied unsteady boundary-layer flow around a sphere. Huang and Chen [16] solved the laminar free-convection flow about a sphere with surface blowing and suction effects, while Lien et al. [17] considered mixed and free convection over a rotating sphere with wall suction and blowing.

For many years, a significant number of investigations have been carried out on the effects of electrically conducting fluids such as liquid metals in the presence of a magnetic field on the flow and heat transfer aspects (for example, Sparrow and Cess [18], Riley [19], Michiyoshi, Takahashi and Serizawa [20], Gray [21], and Fumizawa [22]). Vajravelu and Nayfeh [23] obtained similarity solutions for hydromagnetic free convection at a cone and a wedge. Aldoss and Ali [24] have recently considered mixed convection from a horizontal cylinder with suction and blowing in the presence of a magnetic field. In addition, Yih [25] studied the effects of viscous and Joule heating on magnetohydrodynamic (MHD) natural-convection flow over a permeable sphere in porous media.

The coupled heat and mass transfer problem has received relatively little attention. Brunn [26] studied heat or mass transfer from a sphere in a low-Reynolds-number flow. Feng and Michaelides [27] reported on mass and heat transfer from spheres at low Reynolds numbers. Yucel [28] considered coupled heat and mass transfer about a vertical cylinder in porous media. Lai and Kulacki [29] investigated coupled heat and mass transfer by natural convection from a sphere embedded in porous media. Recently, Yih [30] considered coupled heat and mass transfer by natural convection adjacent to a permeable horizontal cylinder in a saturated porous medium.

Motivated by the investigations mentioned above, the purpose of the present work is to consider simultaneous heat and mass transfer by natural-convection flow around a permeable sphere maintained at uniform heat and mass fluxes in the presence of magnetic field and thermal radiation effects.

GOVERNING EQUATIONS

Consider coupled heat and mass transfer by hydromagnetic natural convection from a permeable sphere in the presence of thermal radiation effects. A uniform magnetic field is applied in the direction normal to the surface. The surface of the cylinder is maintained at a uniform heat flux q_w and a uniform mass flux m_w. Far from the sphere surface, the free stream is kept at a constant temperature T_∞ and a constant concentration c_∞. Constant fluid suction or injection is imposed at the surface of the sphere. The flow model and physical coordinate system are shown in Figure 1. The fluid is assumed to be Newtonian, viscous, electrically conducting, gray, and absorbing/emitting radiation, but nonscattering. The Rosseland

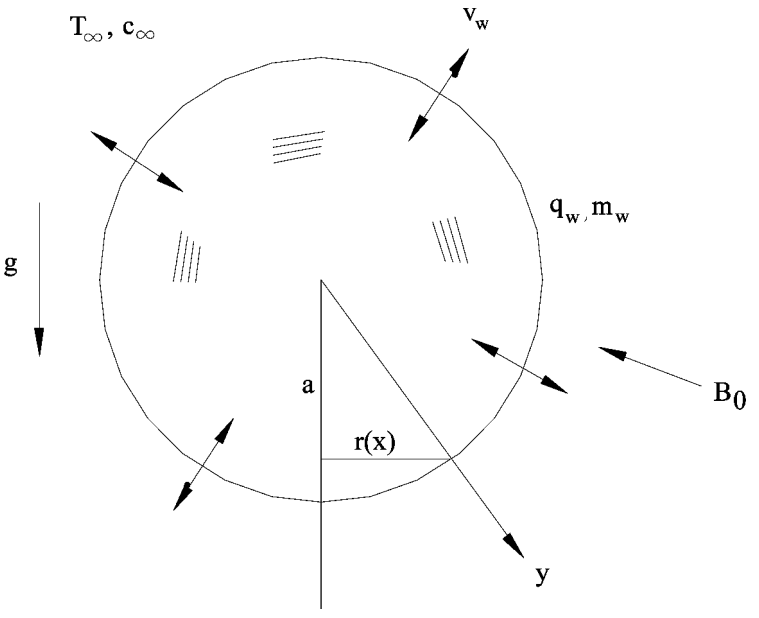

Figure 1. Flow model and physical coordinate system.

approximation is assumed to be valid to represent the radiative heat flux in the energy equation. The surface of the sphere is assumed to be electrically insulating. All fluid properties are assumed constant except the density in the buoyancy term of the x-momentum equation. The magnetic Reynolds number is assumed to be small, so that the induced magnetic field is neglected. In addition, no electric field is assumed to exist, and the Hall effect is negligible. In the absence of an electric field, the small magnetic Reynolds number assumption uncouples Maxwell's equations from the Navier-Stokes equations (Cramer and Pai [31]). Taking all of the above assumptions into consideration and invoking the boundary-layer and Boussinesq approximations, the governing equations can be written in dimensional form as

$$\frac{\partial(ru)}{\partial x}+\frac{\partial(rv)}{\partial y}=0 \tag{1}$$

$$u\frac{\partial u}{\partial x}+v\frac{\partial u}{\partial y}=\nu\frac{\partial^2 u}{\partial y^2}+g\sin\left(\frac{x}{a}\right)[\beta_T(T-T_\infty)+\beta_c(c-c_\infty)]-\frac{\sigma B_0^2}{\rho}u \tag{2}$$

$$u\frac{\partial T}{\partial x}+v\frac{\partial T}{\partial y}=\frac{\nu}{\mathrm{Pr}}\frac{\partial^2 T}{\partial y^2}-\frac{1}{\rho c_p}\frac{\partial q_r}{\partial y} \tag{3}$$

$$u\frac{\partial c}{\partial x}+v\frac{\partial c}{\partial y}=D\frac{\partial^2 c}{\partial y^2} \tag{4}$$

where x, y, and r are the circumferential or streamwise, the transverse distances, and the radial distance from the symmetric axis to surface, respectively. $r=a[\sin(x/a)]$, where a is the radius of the sphere. The symbols u, v, T, and c are the fluid x component of velocity, the y component of velocity, temperature, and concentration, respectively. ρ, ν, c_p, Pr, β_T, and β_c are the fluid density, kinematic viscosity, specific heat at constant pressure, Prandtl number, coefficient of thermal expansion, and coefficient of concentration of expansion, respectively. σ, B_0, D, and q_r are the electrical conductivity, magnetic induction, mass diffusivity, and radiative heat flux, respectively. g, T_∞, and c_∞ are the acceleration due to gravity and the free-stream temperature and concentration, respectively.

The boundary conditions for this problem are given by

$$\begin{aligned} &y=0\text{: } v=v_w \qquad q_w=-k\frac{\partial T}{\partial y} \qquad m_w=-D\frac{\partial c}{\partial y}\\ &y\to\infty\text{: } u=0 \qquad T=T_\infty \qquad c=c_\infty \end{aligned} \tag{5}$$

where v_w is the suction (<0) or injection (>0) velocity and k is the fluid thermal conductivity.

In addition, the radiative heat flux q_r is described according to the Rosseland approximation such that

$$q_r=-\frac{4\sigma_1}{3K_1}\frac{\partial T^4}{\partial y} \tag{6}$$

where σ_1 and K_1 are the Stefan-Boltzmann constant and the mean absorption coefficient, respectively. As done by Raptis [32, 33], the fluid-phase temperature differences within the flow are assumed to be sufficiently small so that T^4 may be expressed as a linear function of temperature. This is done by expanding T^4 in a Taylor series about the free-stream temperature T_∞ and neglecting higher-order terms to yield

$$T^4 = 4T_\infty^3 T - 3T_\infty^4 \tag{7}$$

By using Eqs. (6) and (7) in the last term of Eq. (3), one obtains

$$\frac{\partial q_r}{\partial y} = -\frac{16\sigma_1 T_\infty^3}{3K_1}\frac{\partial^2 T}{\partial y^2} \tag{8}$$

It is convenient to transform Eqs. (1)–(5) by using the following nonsimilarity transformations reported earlier by Yih [25]:

$$\begin{gathered} \xi = \frac{x}{a} \qquad \eta = \frac{y}{a}(\mathrm{Gr})^{1/5} \qquad \psi = \nu\xi(\mathrm{Gr})^{1/5} f(\xi,\eta) \\ \theta(\xi,\eta) = \frac{k(\mathrm{Gr})^{1/5}(T-T_\infty)}{aq_w} \qquad C(\xi,\eta) = \frac{D(\mathrm{Gr})^{1/5}(c-c_\infty)}{am_w} \end{gathered} \tag{9}$$

where $\mathrm{Gr} = g\beta_T q_w a^4/(k\nu^2)$ is the Grashof number and ψ is the dimensional stream function defined in the usual way as $ru = \partial(r\psi)/\partial y$ and $rv = -\partial(r\psi)/\partial x$ so that the continuity equation is identically satisfied. In terms of the above variables,

$$u = \frac{\nu(\mathrm{Gr})^{2/5}}{a}\xi f' \qquad v = -\frac{\nu(\mathrm{Gr})^{1/5}}{a}\left[\xi\frac{\partial f}{\partial \xi} + \left(1 + \frac{\xi\cos(\xi)}{\sin(\xi)}\right)f\right] \tag{10}$$

Substituting Eqs. (9) into Eqs. (1)–(5) [taking Eq. (8) into account] yields the following nonsimilar equations and boundary conditions:

$$f''' + \left[1 + \frac{\xi\cos(\xi)}{\sin(\xi)}\right]ff'' - (f')^2 + \frac{\sin\xi}{\xi}(\theta + NC) - \mathrm{Ha}^2 f' = \xi\left(f'\frac{\partial f'}{\partial\xi} - f''\frac{\partial f}{\partial\xi}\right) \tag{11}$$

$$\frac{1}{\mathrm{Pr}}\left(1 + \frac{4}{3N_R}\right)\theta'' + \left[1 + \frac{\xi\cos(\xi)}{\sin(\xi)}\right]f\theta' = \xi\left(f'\frac{\partial\theta}{\partial\xi} - \theta'\frac{\partial f}{\partial\xi}\right) \tag{12}$$

$$\frac{C''}{\mathrm{Sc}} + \left[1 + \frac{\xi\cos(\xi)}{\sin(\xi)}\right]fC' = \xi\left(f'\frac{\partial C}{\partial\xi} - C'\frac{\partial f}{\partial\xi}\right) \tag{13}$$

$$\begin{gathered} \eta = 0: \qquad f' = 0 \qquad \xi\frac{\partial f}{\partial\xi} + \left[1 + \frac{\xi\cos(\xi)}{\sin(\xi)}\right]f = f_0 \qquad \theta' = -1 \qquad C' = -1 \\ \eta \to \infty: \qquad f' = 0 \qquad \theta = 0 \qquad C = 0 \end{gathered} \tag{14}$$

where

$$\mathrm{Ha}^2 = \frac{\sigma B_0^2 a^2}{\rho \nu (\mathrm{Gr})^{2/5}} \qquad N_R = \frac{kK_1}{4\sigma_1 T_\infty^3} \qquad N = \frac{\beta_c m_w / D}{\beta_T q_w / k}$$
$$\mathrm{Sc} = \frac{\nu}{D} \qquad f_0 = -\frac{\nu_w a}{\nu (\mathrm{Gr})^{1/5}} \tag{15}$$

are the square of the Hartmann number, dimensionless radiation parameter, buoyancy ratio, Schmidt number, and the dimensionless suction ($f_0 > 0$) or injection ($f_0 < 0$) velocity.

At $\xi = 0$, the following similarity equations and boundary conditions are obtained:

$$f''' + 2ff'' - (f')^2 + \theta + NC - \mathrm{Ha}^2 f' = 0 \tag{16}$$

$$\frac{1}{\mathrm{Pr}}\left(1 + \frac{4}{3N_R}\right)\theta'' + 2f\theta' = 0 \tag{17}$$

$$\frac{C''}{\mathrm{Sc}} + 2fC' = 0 \tag{18}$$

$$\eta = 0: \qquad f' = 0 \qquad f = \frac{f_0}{2} \qquad \theta' = -1 \qquad C' = -1$$
$$\eta \to \infty: \quad f' = 0 \qquad \theta = 0 \qquad C = 0 \tag{19}$$

The skin-friction coefficient and the Nusselt and Sherwood numbers can be computed from the following relations:

$$C_f = \frac{\tau_w}{\rho(\nu/a)^2 (\mathrm{Gr})^{3/5}} = \xi f''(\xi, 0) \tag{20}$$

$$\mathrm{Nu} = \frac{ha}{k} = (\mathrm{Gr})^{1/5} \frac{1}{\theta(\xi, 0)} \qquad \text{or} \qquad \mathrm{Nu}(\mathrm{Gr})^{-1/5} = \frac{1}{\theta(\xi, 0)} \tag{21}$$

$$\mathrm{Sh} = \frac{h_m a}{D} = (\mathrm{Gr})^{1/5} \frac{1}{C(\xi, 0)} \qquad \text{or} \qquad \mathrm{Sh}(\mathrm{Gr})^{-1/5} = \frac{1}{C(\xi, 0)} \tag{22}$$

where τ_w, h, and h_m are the wall shear stress and the heat and mass transfer coefficients, respectively.

NUMERICAL METHOD

The nonsimilar equations (11)–(13) are linearized and then descritized using three points central difference quotients with variable step sizes in the η direction and using two-point backward difference formulas in the ξ direction with a constant

step size. The resulting equations form a tri-diagonal system of algebraic equations that can be solved by the well-known Thomas algorithm (see Blottmer [34]). The solution process starts at $\xi = 0$, where Eqs. (16)–(18) are solved, and then marches forward using the solution at the previous line of constant ξ until it reaches the desired value of ξ (=120° in this case). Due to the nonlinearities of the equations, an iterative solution with successive over- or underrelaxation techniques is required. The convergence criterion required that the maximum absolute error between two successive iterations be 10^{-6}. The computational domain was made of 196 grids in the η direction and 1,000 grids in the ξ direction. A starting step size of 0.001 in the η direction with an increase of 1.0375 times the previous step size and a constant step size in the ξ direction of 0.0021 were found to give very accurate results. The maximum value of η, which represented the ambient conditions, was assumed to be 35. The step sizes employed were arrived at after performing numerical experimentations to assess grid independence and ensure accuracy of the results. The accuracy of the aforementioned numerical method was validated by direct comparisons with the numerical results reported earlier by Huang and Chen [16], Chiang et al. [35], Lien et al. [17], and Yih [25] in the absence of magnetic field, and thermal radiation and concentration buoyancy effects. Tables 1–4 present the results of these various comparisons. It can be seen from these tables that excellent agreement between the results exists. These favorable comparisons lend confidence in the numerical results to be reported in the next section.

RESULTS AND DISCUSSION

In this section, a representative set of graphical results for the dimensionless velocity $f'(\xi, \eta)$, temperature $\theta(\xi, \eta)$, and concentration $C(\xi, \eta)$, as well as the local skin-friction coefficient $C_f(\xi)$, local wall temperature $\theta(\xi, 0)$, and local wall concentration $C(\xi, 0)$, is presented and discussed for various parametric conditions. These conditions are intended for two electrically conducting fluids, metal ammonia suspensions ($\mathrm{Pr} = 0.78$) and mercury ($\mathrm{Pr} = 0.027$) polluted by water vapor ($\mathrm{Sc} = 0.6$), in the presence of a magnetic field and thermal radiation effects.

Figures 2–4 display typical profiles for the dimensionless velocity, temperature, and concentration at the circumferential position $\xi = 90°$ for various values of the buoyancy ratio N and two values of the Hartmann number Ha, respectively. For $N = 0$ the flow around the sphere is induced only by thermal buoyancy effect due to

Table 1. Comparison of $f''(\xi, 0)$ for various values of Pr with $f_0 = 0$, $\mathrm{Ha} = 0$, $N = 0$, and $N_R = \infty$

Pr	ξ	Huang and Chen [16]	Yih [25]	Present results
0.7	0°	1.2276	1.2278	1.2273
	30°	1.2031	1.2032	1.2023
	60°	1.1296	1.1297	1.1288
	90°	1.0071	1.0072	1.0065
7.0	0°	0.5165	0.5159	0.5157
	30°	0.5065	0.5059	0.5058
	60°	0.4768	0.4762	0.4761
	90°	0.4276	0.4271	0.4271

Table 2. Comparison of $\theta(\xi, 0)$ for various values of Pr with $f_0 = 0$, Ha = 0, $N = 0$, and $N_R = \infty$

Pr	ξ	Chiang et al. [35]	Lien et al. [17]	Huang and Chen [16]	Yih [25]	Present results
0.7	0°	1.8691	1.8700	1.8700	1.8689	1.8683
	30°	1.8913	1.8931	1.8927	1.8917	1.8902
	60°	1.9582	1.9653	1.9648	1.9638	1.9628
	90°	2.0696	2.1026	2.1018	2.1004	2.0989
7.0	0°	—	—	1.0350	1.0354	1.0341
	30°	—	—	1.0477	1.0481	1.0471
	60°	—	—	1.0879	1.0884	1.0872
	90°	—	—	1.1642	1.1649	1.1636

the temperature gradient. However, for $N > 0$ the flow around the sphere is caused by both temperature and concentration gradients. In this case, the flow will be aided by the concentration buoyancy effects. Therefore, as N increases, the flow around the sphere increases at the expense of decreased temperature and concentration. These decreases in both the temperature and concentration values are followed by corresponding decreases in both the thermal and solutal (concentration) boundary layers. These behaviors are clearly shown in Figures 2–4. Furthermore, imposition of a magnetic field to an electrically conducting fluid creates a draglike force called the Lorentz force. This force has the tendency to slow down the flow around the sphere at the expense of increasing its temperature and concentration. This is depicted by the decreases in the velocity values and increases in the temperature and concentration values as Ha increases shown in Figures 2–4. In addition, the increases in the temperature and concentration values as Ha increases are accompanied by increases in both the thermal and concentration boundary layers. The behaviors explained in Figures 2–4 are for $\xi = 90°$ and are also applicable for every other circumferential position ξ.

Figures 5–7 illustrate the behavior of the distributions of the local skin-friction coefficient $C_f(\xi)$, local wall temperature $\theta(\xi, 0)$ (reciprocal of local Nusselt number), and local wall concentration $C(\xi, 0)$ (reciprocal of local Sherwood number) due to changes in the values of Ha and N, respectively. In general, as the circumferential position ξ increases, all of $C_f(\xi)$, $\theta(\xi, 0)$, $C(\xi, 0)$ increase. As mentioned before and seen from Figures 3 and 4, for a given Hartmann number, increasing the buoyancy

Table 3. Comparison of $f''(\xi, 0)$ for various values of f_0 and Pr with Ha = 0, $N = 0$, and $N_R = \infty$

Pr	ξ	Huang and Chen [16] $f_0 = -0.8$	Huang and Chen [16] $f_0 = 0.8$	Yih [25] $f_0 = -0.8$	Yih [25] $f_0 = 0.8$	Present results $f_0 = -0.8$	Present results $f_0 = 0.8$
0.7	0°	1.5635	0.8946	1.5635	0.8948	1.5617	0.8940
	30°	1.5294	0.8761	1.5293	0.8765	1.5278	0.8757
	60°	1.4262	0.8217	1.4260	0.8220	1.4250	0.8213
	90°	1.2515	0.7341	1.2515	0.7344	1.2510	0.7337
7.0	0°	2.9668	0.0317	2.9594	0.0321	2.9535	0.0319
	30°	2.9032	0.0303	2.8946	0.0307	2.8921	0.0303
	60°	2.7086	0.0263	2.7000	0.0268	2.6899	0.0263
	90°	2.3767	0.0203	2.3685	0.0208	2.3666	0.0203

Table 4. Comparison of $\theta(\xi, 0)$ for various values of f_0 and Pr with $\mathrm{Ha} = 0$, $N = 0$, and $N_R = \infty$

Pr	ξ	Huang and Chen [16] $f_0 = -0.8$	Huang and Chen [16] $f_0 = 0.8$	Yih [25] $f_0 = -0.8$	Yih [25] $f_0 = 0.8$	Present results $f_0 = -0.8$	Present results $f_0 = 0.8$
0.7	0°	2.9107	1.2186	2.9093	1.2179	2.9054	1.2172
	30°	2.9516	1.2295	2.9498	1.2290	2.9473	1.2284
	60°	3.0806	1.2642	3.0783	1.2639	3.0767	1.2633
	90°	3.3231	1.3301	3.3194	1.3303	3.3173	1.3287
7.0	0°	7.3045	0.1784	7.2667	0.1784	7.2466	0.1787
	30°	7.3817	0.1784	7.3404	0.1784	7.3217	0.1787
	60°	7.6120	0.1785	7.5701	0.1786	7.5600	0.1788
	90°	8.0116	0.1786	7.9686	0.1789	7.9494	0.1789

ratio causes the temperature and concentration at the sphere surface to decrease at every circumferential position ξ. This behavior results in increases in both the local Nusselt and local Sherwood numbers according to Eqs. (21) and (22). Also, as N increases, the wall slope of the velocity profile $f''(\xi, 0)$ increases and, based on Eq. (20), the values of $C_f(\xi)$ increase. However, as Ha increases, $f''(\xi, 0)$ decreases [resulting in decreases in the values of $C_f(\xi)$] while both of $\theta(\xi, 0)$ and $C(\xi, 0)$ increase, as is clear from Figures 5–7.

Figures 8–10 present the effects of the suction or injection parameter f_0 on the velocity, temperature, and concentration profiles at $\xi = 90°$ for two values of the Prandtl number Pr corresponding to metal ammonia suspensions ($\mathrm{Pr} = 0.78$) and mercury ($\mathrm{Pr} = 0.027$), respectively. For a given value of Pr, imposition of wall fluid suction ($f_0 > 0$) tends to deccelerate the flow around the sphere, with reduced temperature and concentration profiles. On the other hand, imposition of fluid

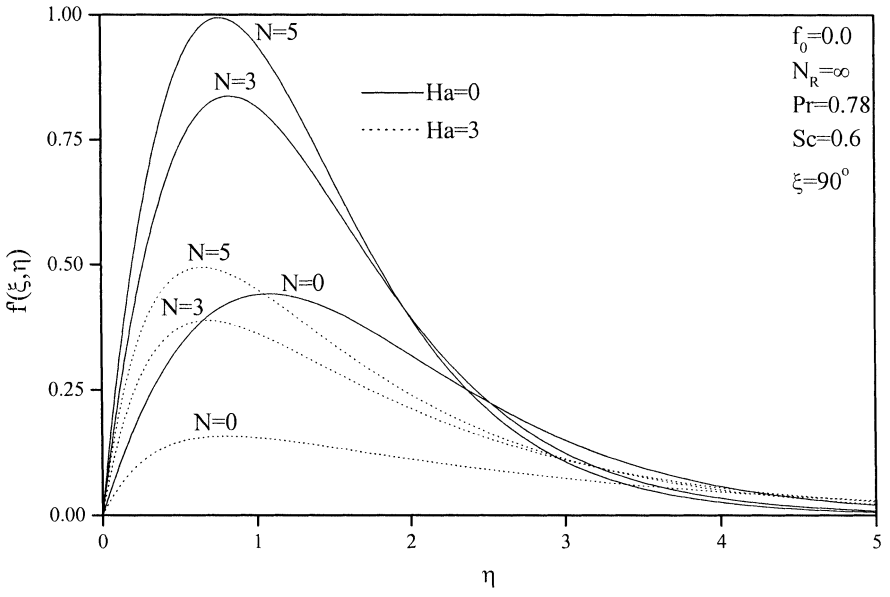

Figure 2. Effects of Ha and N on velocity profiles.

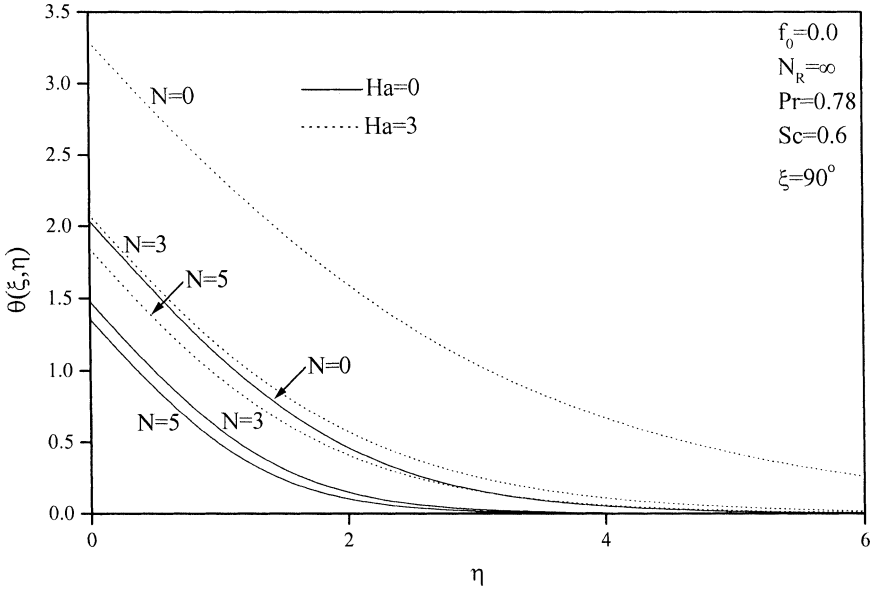

Figure 3. Effects of Ha and N on temperature profiles.

injection or blowing at the sphere surface ($f_0 < 0$) produces the opposite behavior, namely, an increase in the flow velocity and increases in the temperature and concentration, as depicted in Figures 8–10. Furthermore, it is observed from these figures that for a given value of f_0, both the velocity and temperature profiles as well

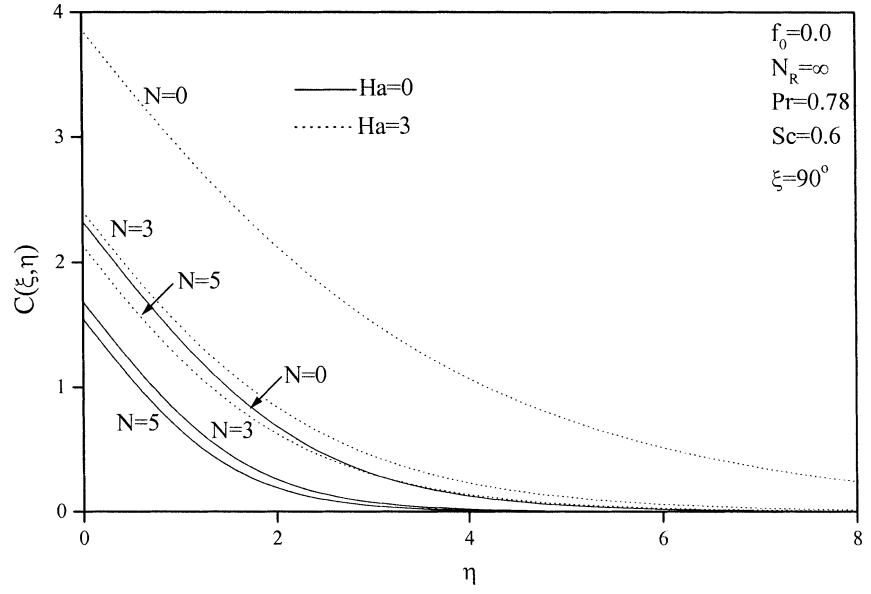

Figure 4. Effects of Ha and N on concentration profiles.

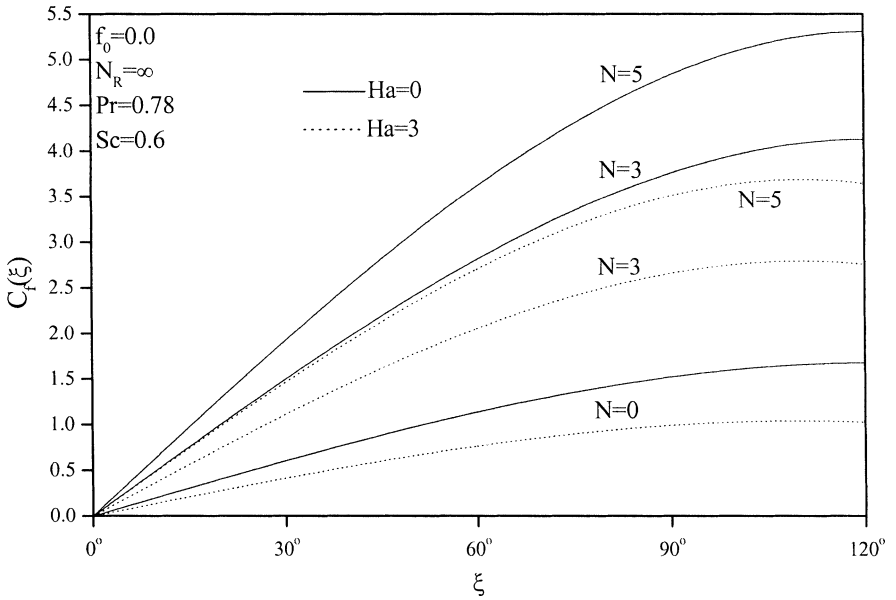

Figure 5. Effects of Ha and N on local skin-friction coefficient.

as their boundary layers increase, while the concentration profile and its boundary layer decrease as Pr decreases.

In Figures 11–13, the effects of f_0 and Pr on $C_f(\xi)$, $\theta(\xi, 0)$, $C(\xi, 0)$ are presented, respectively. In these figures, it is predicted that, regardless of the value of

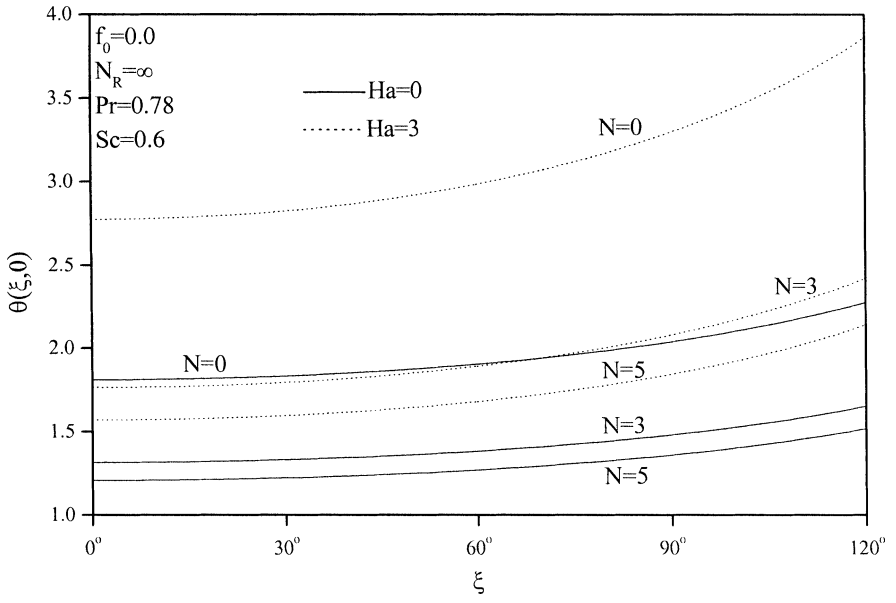

Figure 6. Effects of Ha and N on local wall temperature.

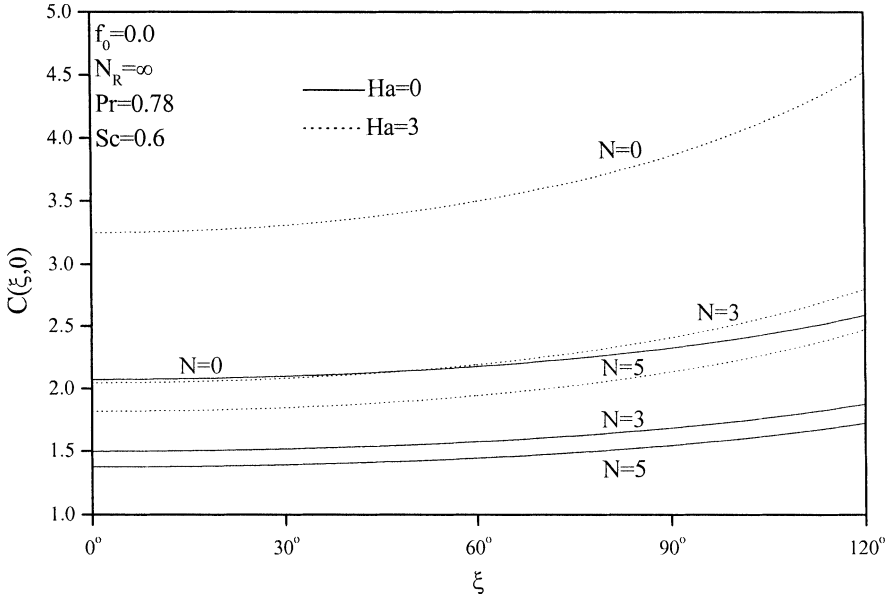

Figure 7. Effects of Ha and N on local wall concentration.

Pr, both $\theta(\xi, 0)$, $C(\xi, 0)$ decrease as the suction/injection parameter f_0 increases. However, this is not the case for $C_f(\xi)$, since it decreases for $\Pr = 0.78$ and increases for $\Pr = 0.027$ as f_0 increases. This can be explained from Figure 8, where it is clearly seen that for $\Pr = 0.027$, the wall slopes of the velocity profiles become steep and

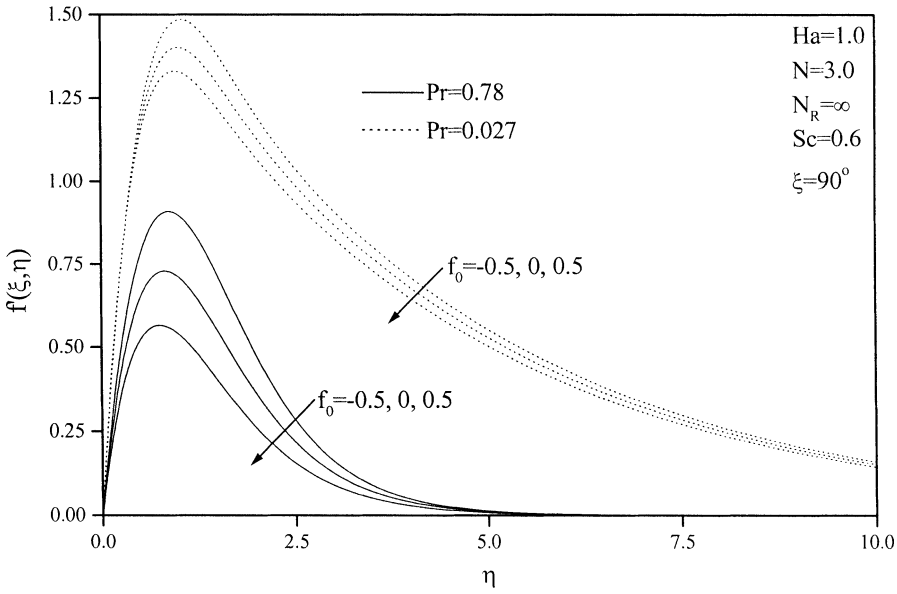

Figure 8. Effects of f_0 and Pr on velocity profiles.

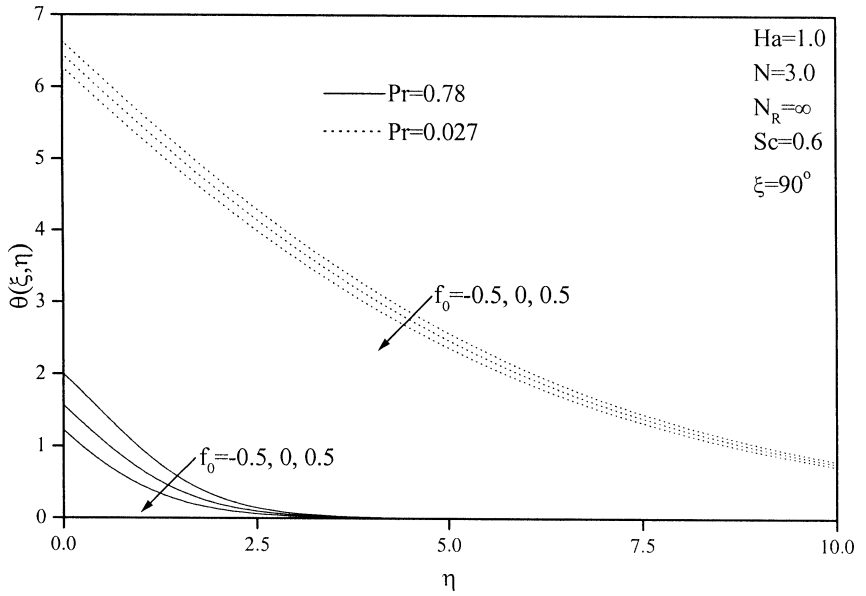

Figure 9. Effects of f_0 and Pr on temperature profiles.

slightly increased as f_0 increases, while they are clearly reduced for $\mathrm{Pr} = 0.78$. The effect of reducing the value of Pr is observed to increase the values of both $C_f(\xi)$, $\theta(\xi, 0)$ and to decrease the values of $C(\xi, 0)$ for all circumferential positions ξ.

Figures 14 and 15 show the influence of the radiation parameter N_R on the local wall temperature and concentration for two values of the Schmidt number Sc,

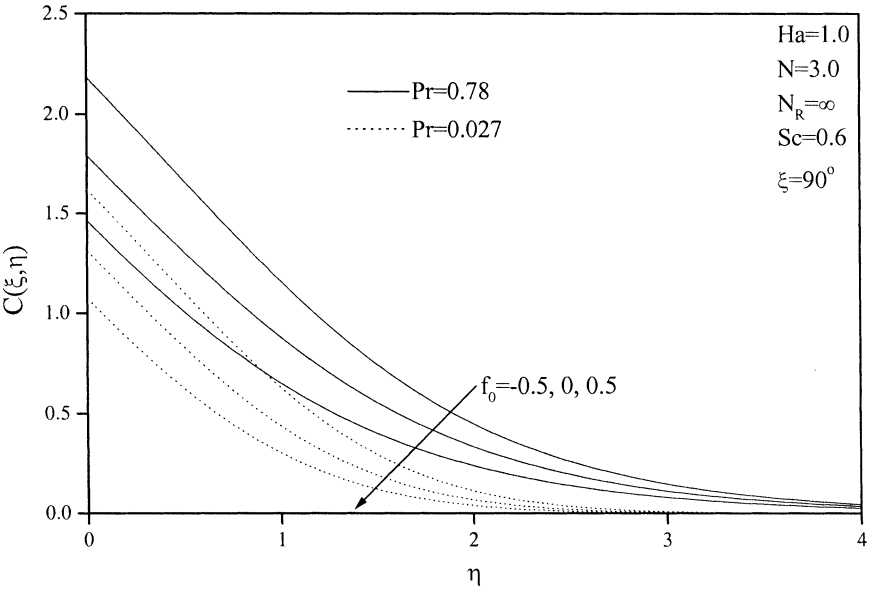

Figure 10. Effects of f_0 and Pr on concentration profiles.

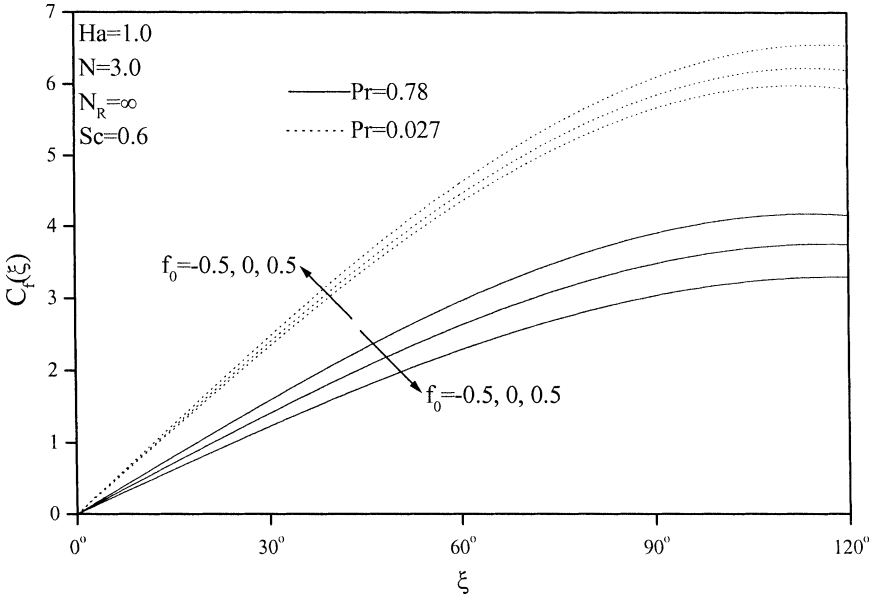

Figure 11. Effects of f_0 and Pr on local skin-friction coefficient.

respectively. In these figures, $N_R = \infty$ corresponds to the case where thermal radiation effects are absent, whereas finite values of N_R indicate that these effects are present. Increases in the radiation effects (decreases in the values of N_R) have the tendency to increase the fluid's thermal state. This causes its wall temperature to

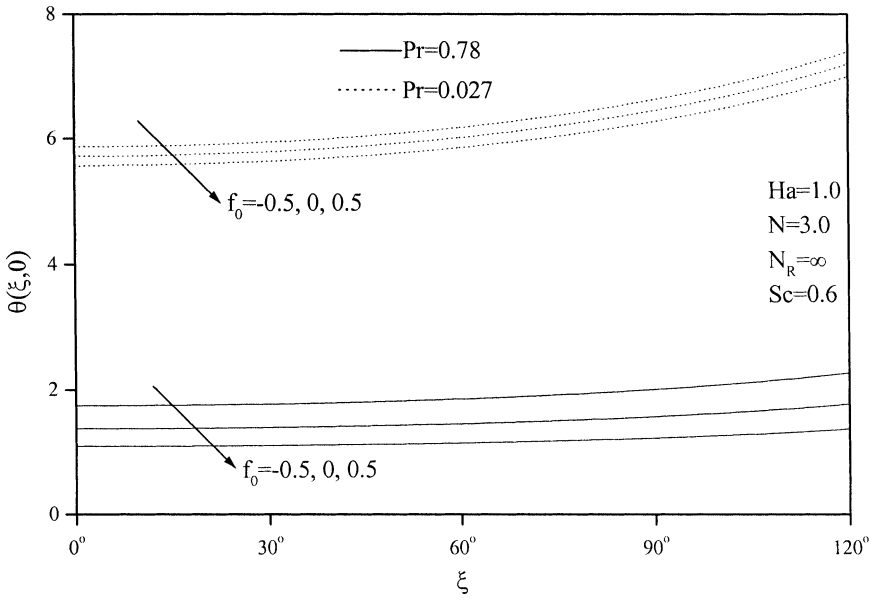

Figure 12. Effects of f_0 and Pr on local wall temperature.

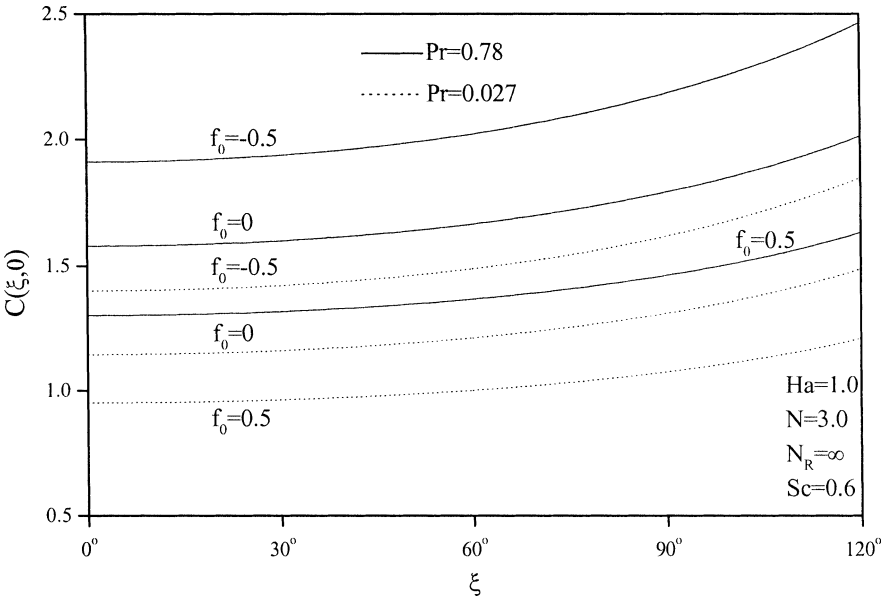

Figure 13. Effects of f_0 and Pr on local wall concentration.

increase as N_R decreases at every circumferential position ξ. This is clear from Figure 14. On the other hand, decreasing the value of N_R has the same effect as increasing the value of Pr on the wall concentration, namely, a decrease in the wall concentration for all values of ξ. This behavior is shown in Figure 15. Furthermore,

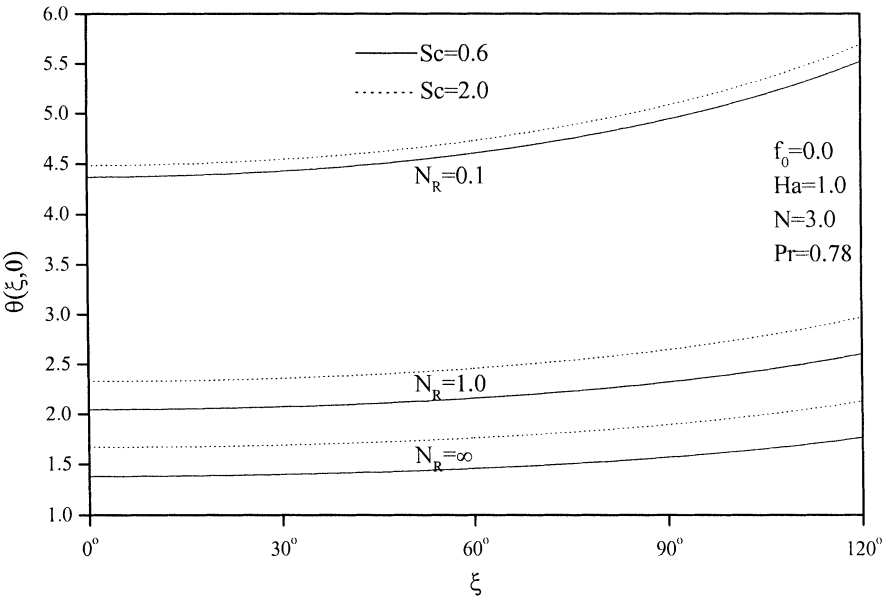

Figure 14. Effects of N_R and Sc on local wall temperature.

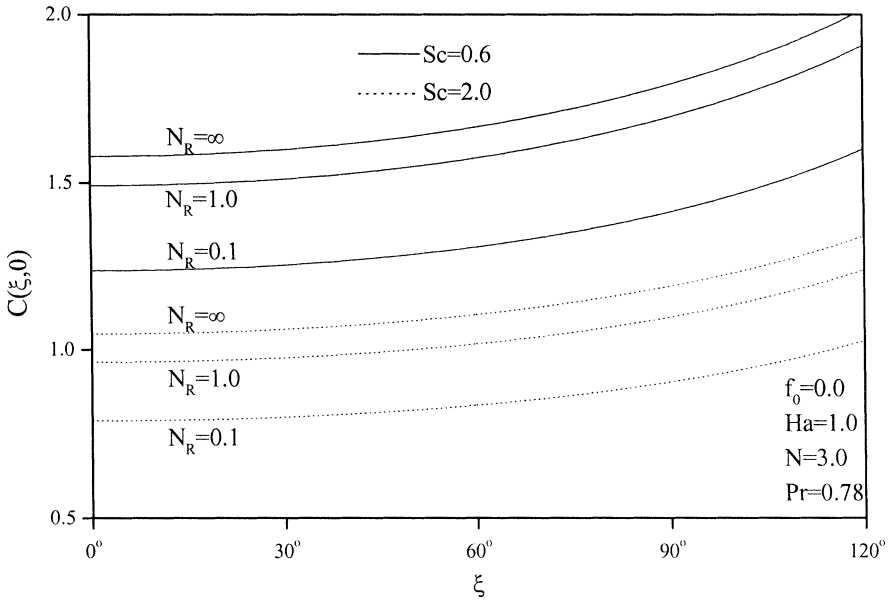

Figure 15. Effects of N_R and Sc on local wall concentration.

for a given value of N_R, increases in the values of the Schmidt number Sc are expected to decrease the concentration profile and its boundary layer and to increase the temperature profile and its boundary layer. This is true for all values of ξ. This results in increasing the values of $\theta(\xi, 0)$ and decreasing the values of $C(\xi, 0)$ as Sc increases. These behaviors are obvious from Figures 14 and 15.

CONCLUSIONS

This work considered coupled heat and mass transfer by natural convection from a sphere in the presence of a magnetic field and thermal radiation effects. The surface of the sphere was maintained at uniform heat and mass fluxes and was permeable so as to allow for fluid wall suction or injection. The governing equations were formulated and transformed into a set of nonsimilar equations. These equations were solved numerically by an implicit, iterative, tri-diagonal, finite-difference method. The obtained results were checked against previously published work and were found to be in excellent agreement. Numerical results for the velocity, temperature, and concentration profiles as well as the local skin-friction coefficient, local wall temperature, and local wall concentration were reported graphically. It was found that both the local wall temperature and local wall concentration (which are the reciprocals of the Nusselt and Sherwood numbers, respectively) decreased due to increases in either the suction/injection parameter or the buoyancy ratio. However, they both increased due to increases in either the Hartmann number or the circumferential position. Also, increases in the values of either of the Prandtl number or the thermal radiation effects (reciprocal of the radiation parameter) produced decreases in the local wall temperature and increases in the local wall concentration.

However, the opposite behavior was predicted as the Schmidt number was increased, where the local wall temperature was increased while the local wall concentration was decreased. Finally, the skin-friction coefficient was increased as either of the buoyancy ratio or the circumferential position increased, and it was decreased due to increases in either the Hartmann number or the Prandtl number. Futhermore, it was observed that the local skin-friction coefficient increased for low values of the Prandtl number such as that for mercury, while it decreased for moderate values of the Prandtl number such as that corresponding to metal ammonia suspensions as the suction/injection parameter was increased. It is hoped that the present work will be useful for validating more complex investigations dealing with heat and mass transfer from spherical bodies.

REFERENCES

1. I. Siekann, The Calculation of the Thermal Boundary Layer on a Rotating Sphere, *Z. Angew. Math. Phys.*, vol. 13, pp. 468–482, 1962.
2. B. T. Chao and R. Grief, Laminar Forced Convection over Rotating Bodies. *J. Heat Transfer*, vol. 96, pp. 463–466, 1974.
3. M. H. Lee, D. R. Jeng, and K. J. De Witt, Laminar Boundary Layer Transfer over Rotating Bodies in Forced Flow, *J. Heat Transfer*, vol. 100, pp. 496–502, 1978.
4. M. Kumari and G. Nath, Nonsimilar Incompressible Boundary Layer Flow over a Rotating Sphere, *Arch. Mech.*, vol. 34, pp. 147–164, 1982.
5. T. S. Chen and A. Mucoglu, Analysis of Mixed Forced and Free Convection about a Sphere, *Int. J. Heat Mass Transfer*, vol. 20, pp. 867–875, 1977.
6. A. Mucoglu and T. S. Chen, Mixed Convection about a Sphere with Uniform Surface Heat Flux, *J. Heat Transfer*, vol. 100, pp. 542–544, 1978.
7. F. E. Fendell, Laminar Natural Convection about an Isothermally Heated Sphere at Small Grashof Numbers, *J. Fluid Mech.*, vol. 34, pp. 163–176, 1968.
8. J. M. Potter and N. Riley, Free Convection from a Heated Sphere at Large Grashof Number, *J. Fluid Mech.*, vol. 100, pp. 769–783, 1980.
9. C. A. Hieber and B. Gebhart, Mixed Convection from a Sphere at Small Reynolds and Grashof Numbers, *J. Fluid Mech.*, vol. 38, pp. 137–159, 1969.
10. N. Riley, The Heat Transfer from a Sphere in Free Convective Flow, *Appl. Math. Lett.*, vol. 9, pp. 41–46, 1996.
11. F. Geoola and A. R. H. Cornish, Numerical Solution of Steady-State Free Convective Heat Transfer from a Solid Sphere, *Int. J. Heat Mass Transfer*, vol. 24, pp. 1369–1379, 1981.
12. F. Geoola and A. R. H. Cornish, Numerical Simulation of Free Convective Heat Transfer from a Sphere, *Int. J. Heat Mass Transfer*, vol. 25, pp. 1677–1687, 1982.
13. H. Jia and G. Gogos, Laminar Natural Convection from Isothermal Spheres, *Int. J. Heat Mass Transfer*, vol. 39, pp. 1603–1615, 1996.
14. S. N. Singh and M. M. Hasan, Free Convection about a Sphere at Small Grashof Number, *Int. J. Heat Mass Transfer*, vol. 26, pp. 781–783, 1983.
15. S. Kocabiyik, An Accelerated Flow around a Sphere, *Comput. Fluids*, vol. 14, pp. 225–237, 1986.
16. M. J. Huang and C. K. Chen, Laminar Free-Convection from a Sphere with Blowing and Suction, *J. Heat Transfer*, vol. 109, pp. 529–532, 1987.
17. F. S. Lien, C. K. Chen, and J. W. Cleaver, Mixed and Free Convection over a Rotating Sphere with Blowing and Suction, *J. Heat Transfer*, vol. 108, pp. 398–404, 1986.

18. E. M. Sparrow and R. D. Cess, Effects of Magnetic Field on Free Convection Heat Transfer, *Int. J. Heat Mass Transfer*, vol. 3, pp. 267–274, 1961.
19. N. Riley, Magnetohydrodynamics Free Convection, *J. Fluid Mech.*, vol. 18, pp. 577–586, 1964.
20. I. Michiyoshi, I. Takahashi, and A. Serizawa, Natural Convection Heat Transfer from a Horizontal Cylinder to Mercury under Magnetic Field, *Int. J. Heat Mass Transfer*, vol. 19, pp. 1021–1029, 1976.
21. D. D. Gray, The Laminar Wall Plume in a Transverse Magnetic Field, *Int. J. Heat Mass Transfer*, vol. 22, pp. 1155–1158, 1979.
22. M. Fumizawa, Natural Convection Experiment with Liquid NaK under Transverse Magnetic Field, *J. Nuclear Sci. Technol.*, vol. 17, pp. 10–17, 1980.
23. K. Vajravelu and J. Nayfeh, Hydromagnetic Convection at a Cone and a Wedge, *Int. Commun. Heat Mass Transfer*, vol. 19, pp. 701–710, 1992.
24. T. K. Aldoss and Y. D. Ali, MHD Free Forced Convection from a Horizontal Cylinder with Suction and Blowing, *Int. Commun. Heat Mass Transfer*, vol. 24, pp. 683–693, 1997.
25. K. A. Yih, Viscous and Joule Heating Effects on Non-Darcy MHD Natural Convection Flow over a Permeable Sphere in Porous Media with Internal Heat Generation, *Int. Commun. Heat Mass Transfer*, vol. 27, pp. 591–600, 2000.
26. P. O. Brunn, Heat or Mass Transfer from Single Spheres in a Low Reynolds Number Flow, *Int. J. Eng. Sci.*, vol. 20, pp. 817–822, 1982.
27. Z. G. Feng and E. E. Michaelides, Mass and Heat Transfer from Spheres at Low Reynolds Numbers, *Powder Technol.*, vol. 112, pp. 63–69, 2000.
28. A. Yucel, Natural Convection of Heat and Mass Transfer along a Vertical Cylinder in a Porous Medium, *Int. J. Heat Mass Transfer*, vol. 33, pp. 2265–2274, 1990.
29. F. C. Lai and F. A. Kulacki, Coupled Heat and Mass Transfer from a Sphere Buried in an Infinite Porous Medium, *Int. J. Heat Mass Transfer*, vol. 33, pp. 209–215, 1990.
30. K. A. Yih, Coupled Heat and Mass Transfer by Natural Convection Adjacent to a Permeable Horizontal Cylinder in a Saturated Porous Medium, *Int. Commun. Heat Mass Transfer*, vol. 26, pp. 431–440, 1999.
31. K. R. Cramer and S. I. Pai, *Magneto Fluid Dynamics for Engineers and Applied Physicists*, McGraw-Hill, New York, 1973.
32. A. Raptis, Flow of a Micropolar Fluid past a Continuously Moving Plate by the Presence of Radiation, *J. Heat Mass Transfer*, vol. 41, pp. 2865–2866, 1998.
33. A. Raptis, Radiation and Free Convection Flow through a Porous Medium, *Int. Commun. Heat Mass Transfer*, vol. 25, pp. 289–295, 1998.
34. F. G. Blottner, Finite-Difference Methods of Solution of the Boundary-Layer Equations, *AIAA J.*, vol. 8, pp. 193–205, 1970.
35. T. Chiang, A. Ossin, and C. L. Tien, Laminar Free Convection from a Sphere, *J. Heat Transfer*, vol. 86, pp. 537–542, 1964.